Acta Crystallographica Section A
Foundations of Crystallography
ISSN 0108-7673

Received 4 January 2001
Accepted 2 February 2001

Approximate solution of the Takagi–Taupin equations for a semi-infinite crystal in the three-beam Laue–Laue case

Gunnar Thorkildsen,[a]* Helge B. Larsen[b] and Edgar Weckert[c]

[a]Department of Mathematics and Natural Science, Stavanger University College, Ullandhaug, N-4091 Stavanger, Norway, [b]Department of Materials Science, Stavanger University College, Ullandhaug, N-4091 Stavanger, Norway, and [c]HASYLAB at DESY, Notkestrasse 85, D-22607 Hamburg, Germany. Correspondence e-mail: gunnar.thorkildsen@tn.his.no

An analytical approximate solution of the Takagi–Taupin equations for a symmetrical three-beam Laue–Laue case in a perfect non-absorbing semi-infinite crystal slab has been obtained. The expression, a second-order expansion, is valid for situations where the effective crystal thickness does not exceed half the actual extinction length and it is shown to be in perfect agreement with the full numerical solution of the fundamental equations.

1. Introduction

Three-beam diffraction has now become a well established tool in the physical estimation of structure-invariant triplet phases, see for instance the review by Weckert & Hümmer (1997). In order to describe the perturbation of the two-beam intensity owing to the gradual excitation of a third lattice node onto the Ewald sphere, the dynamical theory of X-ray diffraction must be used. Up to now, two approaches to the problem have been proposed. The first applies the concepts of Ewald–von Laue fundamental theory (Ewald, 1917; von Laue, 1931), in many cases simplified using the Bethe approximation (Juretschke, 1982*a*,*b*; Høier & Marthinsen, 1983; Juretschke, 1984; Hümmer & Billy, 1986; Chang *et al.*, 1999), or a second-order Born approximation (Chang & Tang, 1988; Chang *et al.*, 1989; Shen, 1998; Stetsko *et al.*, 2000). However, numerical solutions of the fundamental equations eigenvalue problem have also been successfully achieved (Colella, 1974; Chang, 1984; Weckert & Hümmer, 1990; Stetsko & Chang, 1997; Weckert & Hümmer, 1997) and these are essential for evaluating different approximation schemes. Common to all these approaches is the underlying assumption of a semi-infinite plane-parallel perfect-crystal slab as the scattering system.

Another method of attacking the problem is based on the Takagi–Taupin equations (Takagi, 1962, 1969; Taupin, 1964), which naturally deals with crystals of finite size (Thorkildsen, 1987; Thorkildsen & Larsen, 1998; Larsen & Thorkildsen, 1998*a*). So far, solutions of these equations have been obtained only for specific crystal geometries spanned by the involved scattering vectors – *cf.* Figs. 1 and 2 of Thorkildsen & Larsen (1998). The solutions are analytical, expressed as series expansions with a finite number of terms, which make them especially attractive with regard to curve-fitting procedures applied to experimentally measured three-beam profiles. This is important when phase assignments for many low-resolution profiles – obtained for instance with the so-called 'reference-beam' method (Shen, 1998; Chang *et al.*, 1999; Shen *et al.*, 2000) – are to be carried out. The potential of extracting additional information from such refinements will be discussed in a forthcoming paper. A disadvantage of the series-expansion approach is related to its small radius of convergence. In the present work, we present the first important terms in a series expansion of the solution of the Takagi–Taupin equations for a semi-infinite perfect-crystal slab in a symmetrical three-beam transmission (Laue–Laue) case. Furthermore, we demonstrate the equivalence with the numerical solution of the fundamental equations for small crystal thicknesses where it is justified to neglect higher-order terms. The three-beam case $2\bar{2}0/0\bar{2}2/20\bar{2}$ in silicon is used as our working example. The influence of *Pendellösung* effects is also briefly discussed.

2. Theory

The Takagi–Taupin equations for one state of polarization are written in the representation

$$\frac{\partial \tilde{D}_o}{\partial s_o} = i\kappa_{oh}\tilde{D}_h + i\kappa_{og}\tilde{D}_g$$
$$\frac{\partial \tilde{D}_h}{\partial s_h} = i\kappa_{ho}\tilde{D}_o + i\kappa_{hg}\tilde{D}_g$$
$$\frac{\partial \tilde{D}_g}{\partial s_g} = i\kappa_{go}\tilde{D}_o + i\kappa_{gh}\tilde{D}_h.$$

This implies that polarization coupling effects are not taken into account in this work. Furthermore, neither ordinary absorption nor resonant scattering effects are included, *cf.* Larsen & Thorkildsen (1998*a*).

The coordinate s_p is along the wavevector $\mathbf{K}_p$ associated with the diffracted beam $p \in \{o, h, g\}$. $\mathbf{h}$ is regarded as the primary reciprocal-lattice vector and $\mathbf{g}$ the secondary one. The coupling coefficient κ_{pq}, having dimension of inverse length, is related to the structure factor by the relation

$$\kappa_{pq} = (\lambda r_e / V_c) F_{pq} C_{pq}.$$

Here r_e is the classical electron radius, V_c is the volume of the unit cell, λ is the wavelength, F_{pq} is the structure factor associated with the reciprocal-lattice node $p - q$ and C_{pq} is the actual polarization factor for σ or π polarization.

The solution for the displacement field associated with the *primary* diffracted beam at the point P owing to a point source at S, *cf.* Fig. 1, is

$$D_h(P \leftarrow S) = J\tilde{D}_h(\Delta_o, \Delta_h, \Delta_g) \exp(2\pi i \alpha_h \Delta_h) \exp(2\pi i \alpha_g \Delta_g) \times \theta(\Delta_o)\theta(\Delta_h)\theta(\Delta_g) \quad (1)$$

with $\Delta_p = s_p(P) - s_p(S)$. α_h and α_g are excitation errors associated with the $\mathbf{K}_h$ and $\mathbf{K}_g$ beams, respectively. $J = 1/V_s^{(0)}$ is the Jacobian of the transformation from a Cartesian coordinate system to the one defined by the triplet of unit vectors $(\mathbf{s}_o, \mathbf{s}_h, \mathbf{s}_g)$, $\mathbf{s}_p$ being along $\mathbf{K}_p$. The Heaviside unit step functions, $\theta(\Delta_p)$, ensure that the diffracted wave field is zero outside the Borrmann pyramid defined by the unit vectors $\mathbf{s}_p$ with origin at S, *cf.* equation (22) of Thorkildsen & Larsen (1998). For our special case of symmetrical Laue–Laue diffraction, $V_s^{(0)}$, which also corresponds to the volume spanned by $\{\mathbf{s}_p\}$, is given by

$$V_s^{(0)} = 2(3^{1/2}\cos\gamma)\sin^2\theta = \tfrac{3}{2}3^{1/2}\cos\gamma\sin^2\gamma. \quad (2)$$

The angles 2θ and γ are defined by $\angle(\mathbf{s}_p, \mathbf{s}_q) = 2\theta_{pq} = 2\theta$, $\angle(\mathbf{s}_p, \mathbf{n}) = \gamma$; $p, q \in (o, h, g)$. $\mathbf{n}$ is the inward drawn normal to the entrance surface.

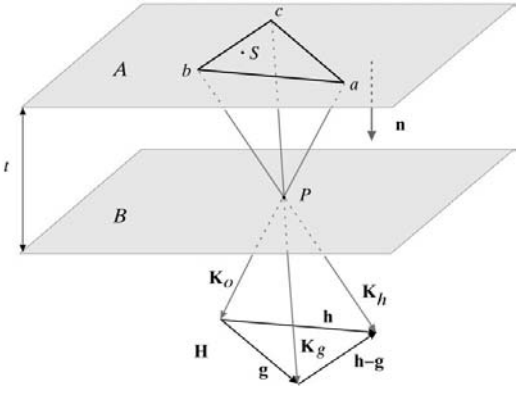

Figure 1
Crystal shaped as a parallel slab of thickness t. A is the entrance surface, B is the exit surface. The actual scattering volume, giving the displacement field at the exit point P, is the inverted Borrmann pyramid $abcP$. The origin of the (s_o, s_h, s_g) coordinate system is located at P. Actual wave vectors $\mathbf{K}_o$. $\mathbf{K}_h$, $\mathbf{K}_g$ all form an angle γ with the inward normal vector $\mathbf{n}$. $\mathbf{h}$, $\mathbf{g}$ and $\mathbf{h} - \mathbf{g}$ are reciprocal-lattice vectors of the primary, secondary and coupling reflections, respectively. The definition of polarization vectors are given in Fig. 2 of Weckert & Hümmer (1997), with the π vectors all lying in the (s_o, s_h) plane.

The displacement field at P is obtained by summing the contributions from all source points within the base abc of the inverted Borrmann pyramid. This also defines the meaning of a semi-infinite crystal in the present context: No Borrmann pyramid as drawn from any source point in the base should be limited by the lateral boundaries of the crystal. The same situation must be true for all exit points as seen by the detector. The calculation is simplified when expressed in an orthonormal coordinate system (r_0, r_1, r_2) with the associated unit base vector $\mathbf{r}_2$ parallel to $\mathbf{n}$. $\mathbf{r}_0$ is along the projection of $\mathbf{s}_g$ onto the exit surface B and $\mathbf{r}_1 = \mathbf{r}_2 \times \mathbf{r}_0$. The origin of this coordinate system is also located at the point P, *cf.* Fig. 2(*a*). In Fig. 2(*b*), the actual ranges of integrations are indicated. We have

$$D_h(P) = (\mathbf{s}_o \cdot \mathbf{n}) \int_{r_0(c)}^{r_0(a)} \mathrm{d}r_0(S) \int_{r_{1x}}^{r_{1y}} \mathrm{d}r_1(S)\, D_h(P \leftarrow S). \quad (3)$$

It is convenient to introduce dimensionless coordinates by redefining r_0 and r_1 according to $r_0 = r_0 t \tan\gamma$ and

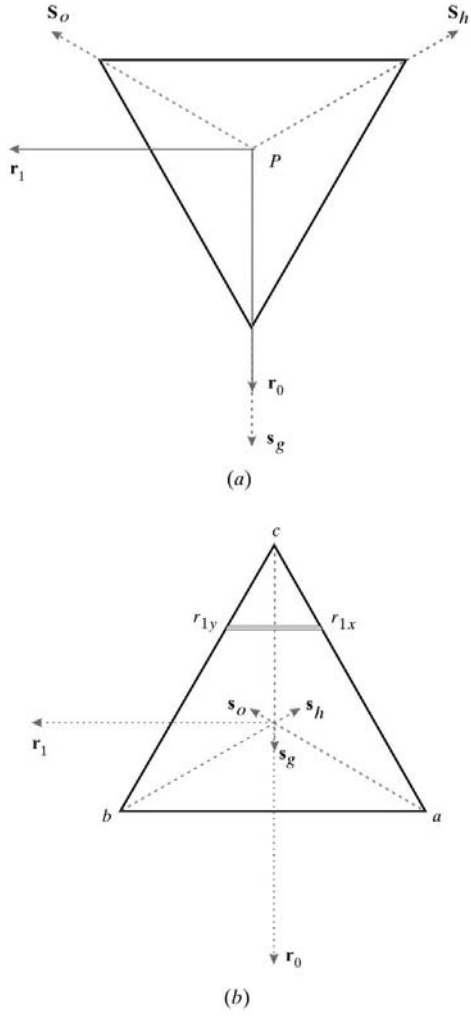

Figure 2
(*a*) Definition of a reference Cartesian coordinate system with the origin at P on the exit surface B. (*b*) abc: area of influence, *i.e.* region for source points, S, on the entrance surface A, contributing to the displacement field at P.

$r_1 = r_1(t/3^{1/2})\tan\gamma$. We then have for the relative coordinates $\{\Delta_p\}$

$$\Delta_o = (\zeta/2)[1 + r_o(S) - r_1(S)],$$
$$\Delta_h = (\zeta/2)[1 + r_o(S) + r_1(S)],$$
$$\Delta_g = (\zeta/2)[1 - 2r_o(S)],$$

where we have defined ζ by

$$\zeta = 2t/(3\cos\gamma).$$

The displacement field of the primary diffracted beam is written as a series expansion

$$\tilde{D}_h(\Delta_o, \Delta_h, \Delta_g) = D_o^{(e)} \sum_{n=1}^{\infty} d_h^{(n)}(\Delta_o, \Delta_h, \Delta_g).$$

$D_o^{(e)}$ is the amplitude associated with the source point. The actual terms, orders 1–3, are

$$d_h^{(1)} = \delta(\Delta_g) = (1/\zeta)\delta[r_o(S) - \tfrac{1}{2}],$$
$$d_h^{(2)} = \Gamma(i\cos\Phi_\Sigma - \sin\Phi_\Sigma),$$
$$d_h^{(3)} = -\Delta_o\Delta_h u\delta(\Delta_g) - \Delta_o v - \Delta_h w.$$

Here, $\Gamma = (\lambda r_e/V_c)(|F_{hg}||F_{go}|/|F_{ho}|)(C_{hg}C_{go}/C_{ho})$ and $\Phi_\Sigma = \varphi_{oh} + \varphi_{hg} + \varphi_{go}$, the phase of the triplet structure invariant. Furthermore, $u = \kappa_{oh}\kappa_{ho}$, $v = \kappa_{og}\kappa_{go}$ and $w = \kappa_{hg}\kappa_{gh}$. We have

$$D_h(P) = \cos\gamma(3^{1/2}/3)(t\tan\gamma)^2 \times \int_{-1}^{1/2} \mathrm{d}r_0(S) \int_{-r_0(S)-1}^{r_0(S)+1} \mathrm{d}r_1(S) D_h(P \leftarrow S). \quad (4)$$

With the following definitions,

$$\alpha = \pi\zeta\alpha_h,$$
$$\beta = \pi\zeta\alpha_g,$$

the intensity, I_h, of the primary diffracted beam, recorded at the point P, is given by equation (25) of Thorkildsen & Larsen (1998):

$$I_h(P) = \frac{c}{2\varepsilon_0}|D_h(P)|^2 = \frac{c}{2\varepsilon_0}\{[\Re D_h(P)]^2 + [\Im D_h(P)]^2\},$$

which, expressed in the variables α and β, becomes to second order

$$I_h(\alpha,\beta) \propto h^{(0)}(\alpha) + \zeta\Gamma\cos\Phi_\Sigma h_1^{(1)}(\alpha,\beta) - \zeta\Gamma\sin\Phi_\Sigma h_2^{(1)}(\alpha,\beta) + \left(\frac{\zeta^2 u}{2}\right)h_1^{(2)}(\alpha) + \left(\frac{\zeta^2 v}{2}\right)h_2^{(2)}(\alpha,\beta) + \left(\frac{\zeta^2 w}{2}\right)h_3^{(2)}(\alpha,\beta) + \zeta^2\Gamma^2 h_3^{(2)}(\alpha,\beta). \quad (5)$$

The functions $\{h\}$ are given in Appendix *A*. The integrated intensity of the primary diffracted beam becomes, using $\alpha_h = (\sin 2\theta/\lambda)\Delta\omega$,

$$\mathcal{I}_h(\beta) = \int \mathrm{d}\Delta\omega\, I_h(\alpha(\Delta\omega),\beta) = \frac{1}{\pi\zeta}\frac{\lambda}{\sin 2\theta}\int \mathrm{d}\alpha\, I_h(\alpha,\beta).$$

Finally, the integrated power

$$\mathcal{P}_h = (\mathbf{s}_h \cdot \mathbf{n})A\mathcal{I}_h(\beta),$$

A being the area of the exit surface as seen by the detector, is expressed by

$$\mathcal{P}_h = \mathcal{P}_h^{(0)}\left\{1 - \tfrac{1}{3}\eta_{oh}^2 - 2\frac{\eta_{hg}\eta_{go}}{\eta_{ho}}\left[f_2(\xi_g)\cos\Phi_\Sigma + f_1(\xi_g)\sin\Phi_\Sigma\right] - 2\left(\eta_{go}^2 + \eta_{hg}^2\right)f_3(\xi_g) + 2\frac{\eta_{hg}^2\eta_{go}^2}{\eta_{ho}^2}f_3(\xi_g)\right\}. \quad (6)$$

$\mathcal{P}_h^{(0)}$ is the kinematical integrated power and we have defined

$$\eta_{pq} = (t/\cos\gamma)(\lambda r_e/V_c)|F_{pq}|C_{pq}, \quad (7)$$
$$\xi_g = 3\beta = 2\pi(t/\cos\gamma)\alpha_g \quad (8)$$

and the shape functions

$$f_1(\xi_g) = (1 - \cos\xi_g)/\xi_g^2, \quad (9)$$
$$f_2(\xi_g) = (\xi_g - \sin\xi_g)/\xi_g^2, \quad (10)$$
$$f_3(\xi_g) = (\xi_g - \sin\xi_g)/\xi_g^3. \quad (11)$$

With $[t] = \mu$m, $[\lambda] = $ Å, $[V_c] = $ Å^3, $[\Delta\omega] = [\Delta\psi] = 10^{-3\circ}$ and $[|\mathbf{h}|] = [|\mathbf{g}|] = $ Å^{-1}, the most important parameters are calculated according to

$$\eta_{pq} = 0.2818[t\lambda/(V_c\cos\gamma)]|F_{pq}|C_{pq},$$
$$\alpha = 0.3655(\cos\theta/\cos\gamma)t|\mathbf{h}|\Delta\omega,$$
$$\beta = 0.3166t|\mathbf{g}|\Delta\psi.$$

$\Delta\omega$ is the angular deviation from the Bragg condition for the primary reflection, while $\Delta\psi$ is the rotation angle for rotation about $\mathbf{h}$ with $\Delta\psi = 0$ corresponding to the exact three-beam point.

For the completely symmetrical case where $\{|F_{pq}|\} = |F|$, *i.e.* $\eta_{pq} = \eta_0 C_{pq}$, we find that the relative change of the integrated power owing to three-beam effects becomes

$$\frac{\Delta\mathcal{P}_h}{\mathcal{P}_h^{(0)}} = -2\left\{\eta_0\frac{C_{hg}C_{go}}{C_{ho}}\left[f_2(\xi_g)\cos\Phi_\Sigma + f_1(\xi_g)\sin\Phi_\Sigma\right] + \eta_0^2\left[(C_{go})^2 + (C_{hg})^2 - \left(\frac{C_{hg}C_{go}}{C_{ho}}\right)^2\right]f_3(\xi_g)\right\}. \quad (12)$$

3. Results and discussion

The key result of the analysis, equation (6), is very similar to what has been obtained for a finite crystal geometry (Thorkildsen & Larsen, 1998). The main differences are related to the shape functions, f_i, emphasizing the different 'weights' put on the terms owing to the particular crystal and scattering geometry. It is important to notice that the phase-carrying terms are associated with the same shape functions in the finite and semi-infinite case.

In order to compare the results based on (12) with numerical calculations based on the fundamental theory, the symmetrical Laue–Laue case $2\bar{2}0/0\bar{2}2/20\bar{2}$ in silicon was chosen as a model system. The inward surface normal is $\mathbf{n} = \bar{1}\bar{1}\bar{1}$. The results presented are for the π-polarization state. The parameters are: $V_c = 160.18$ Å^3, $|F| = 68.711$, $\lambda =$

1.000 Å, $2\theta = 30.188^\circ$, $\gamma = 17.499^\circ$, $|\mathbf{h}| = |\mathbf{g}| = 0.52081$ Å^{-1} and $\Phi_\Sigma = 0.0^\circ$. The polarization factors are calculated according to Weckert & Hümmer (1997) giving $C_{oh} = 0.86438$ and $C_{og} = C_{hg} = -0.96550$.

The three-beam three-dimensional-intensity profile, as calculated from (5), for a crystal plate of thickness 3.0 µm is shown in Fig. 3. Numerical computations were carried out following the procedure devised by Weckert & Hümmer (1997). In this case, the two-beam 'background level' was determined as the average of the integrated power calculated at $\Delta\psi = \pm 0.1^\circ$. Notice that this will be the dynamically integrated power level including primary-extinction effects, while in (12) the kinematically integrated power is used for scaling. When extinction is negligible, as in the cases studied, this will make no difference in the final result.

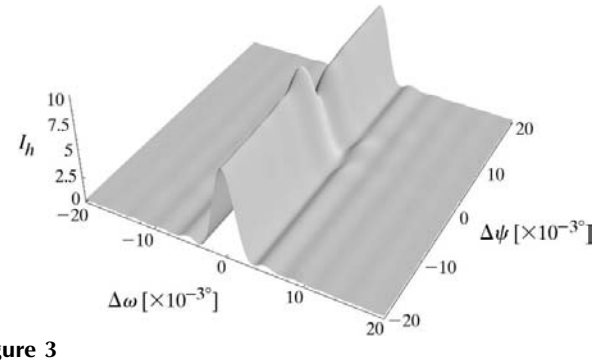

Figure 3
Three-beam three-dimensional intensity profile, π polarization, for the case $2\bar{2}0/0\bar{2}2/20\bar{2}$ in silicon. Crystal thickness $t = 3$ µm. The intensity, I_h, is given in relative units. The angular variables $\Delta\omega$ and $\Delta\psi$ are associated with the orthogonal rotation axes $\hat{\omega}$ and $\hat{\psi}$. A scan in $\Delta\omega$ away from the three-beam situation, $|\Delta\psi| \gg 0$, gives the ordinary two-beam rocking curve of the primary reflection.

A comparison of the two approaches for the relative change in the integrated power for crystal plates of various thicknesses is given in Fig. 4. It is seen that for a small plate thickness the two approaches yield in practice identical results. When t increases, however, the two-term series expansion is no longer valid. This is clearly seen in Fig. 4(*d*), for a plate thickness of 7 µm, where the perturbation of the profile calculated from (12) far exceeds the corresponding result of the numerical calculation. In this case, the η_0 parameter is seen to be above 0.8, indicating a situation of poor convergence. Having a solution to the second order, $\{\eta\}$ parameters should be less than 0.4 in order to ensure valid solutions – *cf.* the discussion in Thorkildsen & Larsen (1998). Absorption, which is not included in the present treatment, is negligible for the plate thicknesses in question ($\Im F_{000} = 1.128$ and $\mu_0 = 39.69\,\mathrm{cm}^{-1}$). The same is true for σ–π polarization coupling as the actual scalar products of polarization vectors are small ($\boldsymbol{\pi}_o \cdot \boldsymbol{\sigma}_g = -\boldsymbol{\pi}_h \cdot \boldsymbol{\sigma}_g = -0.11602$). The inclusion of such effects (and also of asymmetrical scattering situations) would significantly increase the complexity of the solutions (Larsen & Thorkildsen, 1998*a*).

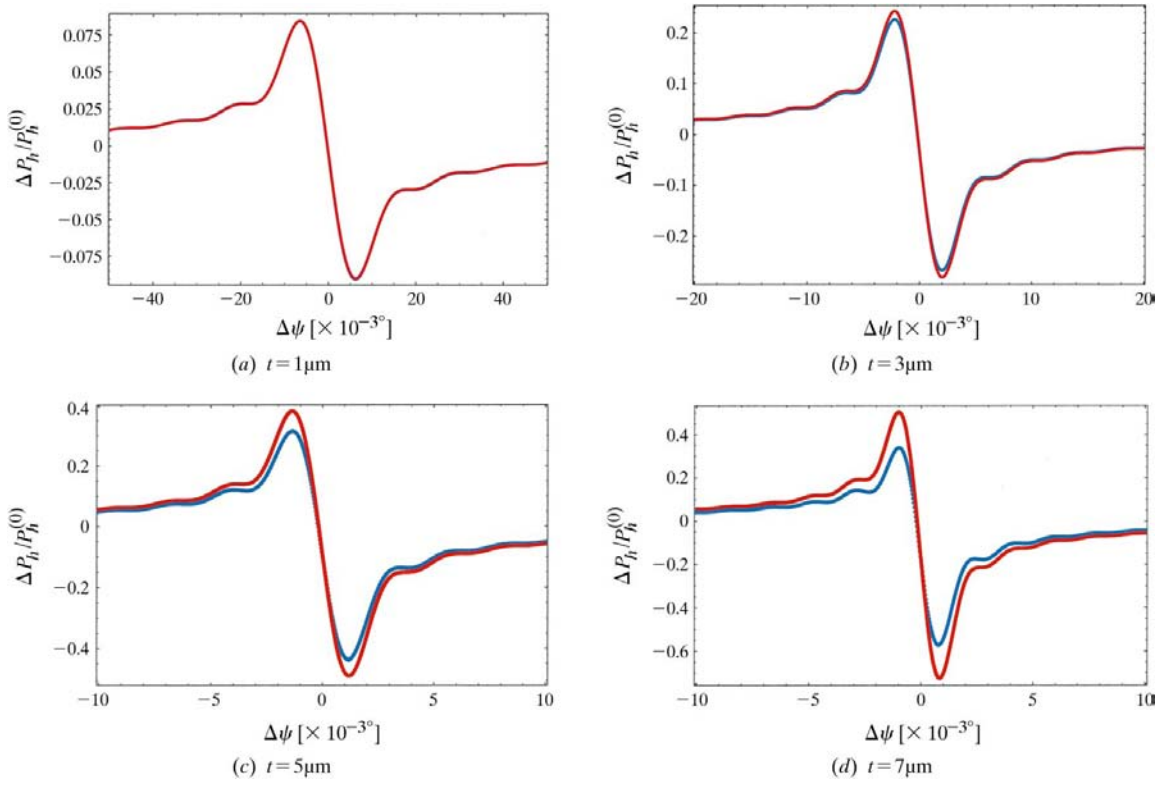

Figure 4
Comparison of simulations based on the Takagi–Taupin formalism (red line) and the calculations from standard plane-wave formalism (blue line) for four different plate thicknesses. Notice the different scales on abscissa and ordinate in the figures. Actual values of η_0 are: $\eta_0 = 0.12675 \times t$[µm]. All figures represent the π-polarization case. The rotation sense of the reciprocal-lattice point **g** is from inside to outside the Ewald sphere, *i.e.* $\Delta\psi < 0$ corresponds to the situation when **g** is inside the sphere.

The numerical calculations also clearly show the danger of using Laue–Laue cases for phase estimations. If the effective crystal thickness as experienced by each of the three beams, $t\cos\gamma$, is larger than the actual 'extinction' lengths $\Lambda_{pq} = 1/|\kappa_{pq}| = 9.5706$ µm, *Pendellösung* effects will become evident and strongly influence the three-beam profiles. An example of this effect for the present three-beam case is depicted in Fig. 5, where the asymmetry of the profile is completely reserved for $t = 20$ µm. These features have already been pointed out by Weckert & Hümmer (1990, 1998). Thus, to use Laue–Laue cases for phase estimations applying the standard scheme of profiles, *cf.* Fig. 6 of Weckert & Hümmer (1997), it is a prerequisite to work with effective crystal thicknesses below one extinction length, leaving us with situations where (6) gives an approximative correct representation of the three-beam perturbation. For thicker crystals, the interpretation becomes much more complicated and may even be untractable.

For a comparison with a real experiment, all theoretical profiles presented have to be convoluted with an experimental resolution function.

4. Concluding remarks

The range of applicability of three-beam diffraction now seems to be divided into two areas. One is concerned with the need for rapid phase assignments for several instantaneous measured profiles, the other with highly resolved profiles probing the sensitivity with regard to various small structural changes. In both cases, the need for well founded analytical solutions is evident. In the former case, phase refinements based on experimentally obtained profiles are pending on a robust and simple, but physically correct, analytical model. In the latter case, the overall effects of different inherent physical parameters on the scattering processes could be better predicted, analyzed and confirmed based on analytical solutions.

The Takagi–Taupin approach has proven successful in this respect. It is capable of handling various crystal shapes and even semi-infinite plates, as shown in the present work. The complementarity with the fundamental theory in a three-beam case, demonstrated for the first time here, shows its generality and potential as a possible 'all-round tool' for analyzing cases when the above simplifying assumptions are fulfilled. In addition, the possibility of formally including crystal imperfection (Larsen & Thorkildsen, 1998*b*) should also be kept in mind.

APPENDIX *A*

A1. Function definitions

The 2D shape functions, expressed in the dimensionless variables α and β, which occur in the definition of the full 3D intensity three-beam profile are given by:

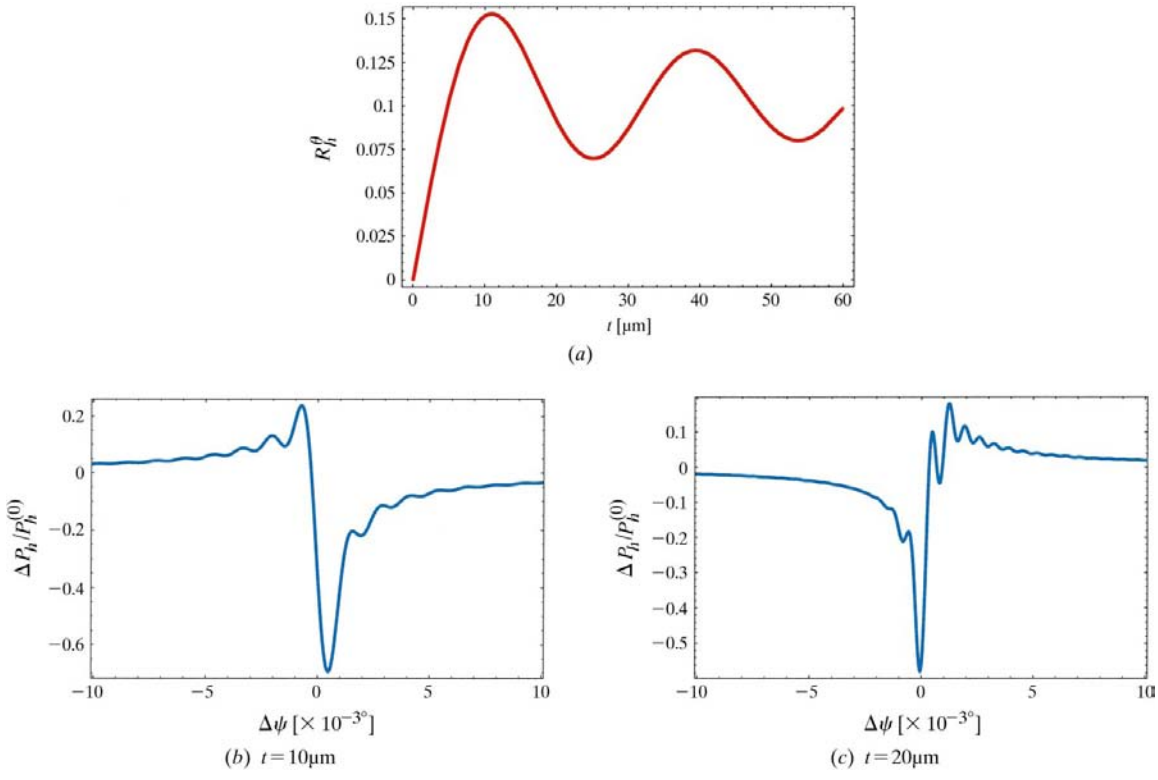

Figure 5
(*a*) Integrated two-beam reflectivity R_h^θ (relative scale) showing the *Pendellösung* effect. (*b*), (*c*) Calculated three-beam profiles from the fundamental theory for $t = 10$ and $t = 20$ µm, respectively, showing the change in shape that might lead to misinterpretation of the value of the triplet phase structure invariant. All figures represent the π-polarization case.

$$h^{(0)}(\alpha) = \frac{4\sin^2(3\alpha/2)}{\alpha^2} = \frac{2(1-\cos 3\alpha)}{\alpha^2}$$

$$h_1^{(1)}(\alpha,\beta) = \big(2\sin(3\alpha/2)\{\alpha\sin[(3\alpha/2)(\alpha-2\beta)] - (\alpha-2\beta)\sin(3\alpha/2)\}\big)/[\alpha^2(\alpha-\beta)\beta]$$

$$h_2^{(1)}(\alpha,\beta) = \frac{-\sin(3\alpha)+\sin[3(\alpha-\beta)]+\sin(3\beta)}{\alpha(\alpha-\beta)\beta}$$

$$h_1^{(2)}(\alpha) = \frac{4\cos(3\alpha)+6\alpha\sin(3\alpha)-4}{\alpha^4}$$

$$h_2^{(2)}(\alpha,\beta) = 2\sin(\tfrac{3}{2}\alpha)\{\alpha^2\sin[\tfrac{3}{2}(\alpha-2\beta)] + 3\alpha(\alpha-\beta)\beta\cos(\tfrac{3}{2}\alpha) - (\alpha^2-2\beta^2)\sin(\tfrac{3}{2}\alpha)\}/[\alpha^3(\alpha-\beta)\beta^2]$$

$$h_3^{(2)}(\alpha,\beta) = 2\sin(\tfrac{3}{2}\alpha)\{-\alpha^2\sin[\tfrac{3}{2}(\alpha-2\beta)] + 3\alpha(\alpha-\beta)\beta\cos(\tfrac{3}{2}\alpha) + (\alpha^2-4\beta\alpha+2\beta^2)\sin(\tfrac{3}{2}\alpha)\}/[\alpha^3(\alpha-\beta)^2\beta]$$

$$h_4^{(2)}(\alpha,\beta) = \{\alpha^2-\beta\alpha-\beta\cos[3(\alpha-\beta)]\alpha + (\beta-\alpha)\cos(3\beta)\alpha + \beta^2+(\alpha-\beta)\beta\cos(3\alpha)\}/[2\alpha^2(\alpha-\beta)^2\beta^2].$$

References

Chang, S.-L. (1984). *Multiple Diffraction of X-rays in Crystals.* Berlin: Springer Verlag.

Chang, S.-L., Chao, C.-H., Huang, Y.-S., Jean, Y.-S., Sheu, H.-S., Liang, F.-J., Chien, H.-C., Chen, C.-K. & Yuan, H. S. (1999). *Acta Cryst.* A**55**, 933–938.

Chang, S.-L., Huang, M.-T., Tang, M.-T. & Lee, C.-H. (1989). *Acta Cryst.* A**45**, 870–878.

Chang, S.-L. & Tang, M.-T. (1988). *Acta Cryst.* A**44**, 1065–1072.

Colella, R. (1974). *Acta Cryst.* A**30**, 413–423.

Ewald, P. P. (1917). *Ann. Phys. (Leipzig)*, **54**, 519–597.

Høier, R. & Marthinsen, K. (1983). *Acta Cryst.* A**39**, 854–860.

Hümmer, K. & Billy, H. (1986). *Acta Cryst.* A**42**, 127–133.

Juretschke, H. J. (1982*a*). *Phys. Rev. Lett.* **48**, 1487–1489.

Juretschke, H. J. (1982*b*). *Phys. Lett.* **92**A, 183–185.

Juretschke, H. J. (1984). *Acta Cryst.* A**40**, 379–389.

Larsen, H. B. & Thorkildsen, G. (1998*a*). *Acta Cryst.* A**54**, 129–136.

Larsen, H. B. & Thorkildsen, G. (1998*b*). *Acta Cryst.* A**54**, 137–145.

Laue, M. von (1931). *Ergebn. exact. Naturwiss.* **10**, 133–158.

Shen, Q. (1998). *Phys. Rev. Lett.* **80**, 3268–3271.

Shen, Q., Kycia, S. & Dobrianov, I. (2000). *Acta Cryst.* A**56**, 268–279.

Stetsko, Y. P. & Chang, S.-L. (1997). *Acta Cryst.* A**53**, 28–34.

Stetsko, Y. P., Juretschke, H. J., Huang, Y.-S., Chao, C.-H., Chen, C.-K. & Chang, S.-L. (2000). *Acta Cryst.* A**56**, 394–400.

Takagi, S. (1962). *Acta Cryst.* **15**, 1311–1312.

Takagi, S. (1969). *J. Phys. Soc. Jpn*, **26**, 1239–1253.

Taupin, D. (1964). *Bull. Soc. Fr. Minéral. Cristallogr.* **87**, 469–511.

Thorkildsen, G. (1987). *Acta Cryst.* A**43**, 361–369.

Thorkildsen, G. & Larsen, H. B. (1998). *Acta Cryst.* A**54**, 120–128.

Weckert, E. & Hümmer, K. (1990). *Acta Cryst.* A**46**, 387–393.

Weckert, E. & Hümmer, K. (1997). *Acta Cryst.* A**53**, 108–143.

Weckert, E. & Hümmer, K. (1998). *Cryst. Res. Technol.* **33**, 653–678.